Journal of Thermal Analysis and Calorimetry (2019) 135:3269–3280
https://doi.org/10.1007/s10973-018-7506-2

Investigation of the bioenergy potential of microalgae *Scenedesmus acuminatus* by physicochemical characterization and kinetic analysis of pyrolysis

José Luiz Francisco Alves[1] · Jean Constantino Gomes Da Silva[1] · Rosangela Lúcio Costa[1] · Seldis Fernando Dos Santos Junior[1] · Valdemar Francisco da Silva Filho[1] · Regina De Fátima Peralta Muniz Moreira[1] · Humberto Jorge José[1]

Received: 5 April 2018 / Accepted: 24 June 2018 / Published online: 29 June 2018

Abstract

In this work, the bioenergy potential of green microalgae *Scenedesmus acuminatus* was evaluated through the psychochemical characteristics and kinetic study of pyrolysis, where the results indicate a good candidate for application in the thermochemical process due to its low moisture and ash content and high calorific value. Its thermal behavior under a heating rate of 10 °C min^{-1} and inert atmosphere shows that decomposition occurs in two stages. Stage I (125–309 °C) involves the pyrolysis of carbohydrates and protein and stage II (309–501 °C) the pyrolysis of lipids. The Starink isoconversional method showed a better application for simulation curves, compared with methods of FWO and KAS. The average values of activated energy were 107.1 and 132.6 kJ mol^{-1} for stages I and II, respectively, which indicates that pyrolysis occurs more easily in stage I than in stage II. The conversion rate curves show that the calculated kinetic parameters are satisfactory for the evaluation of the thermochemical systems.

Keywords Kinetic study · Isoconversional method · Physicochemical characterization · Pyrolysis · *Scenedesmus acuminatus*

Introduction

Biomass is considered to be clean and renewable sources of hydrocarbon that can be used as sustainable fuel. Their advantages are mainly related to growth rate and the ability to fix carbon, which can mitigate environmental problems caused by anthropogenic emissions of greenhouse gases. Different types of biomass have different physiochemical properties and thus different energy potential. In this context, algal biomass represents a promising energy source because of their high rates of growth and carbon-fixing compared with land crops, as well as their low nitrogen and sulfur content [1].

Algae are photosynthetic organisms composed mainly of carbohydrates, lipids and proteins. They are found in saline or freshwater environments and can be generally classified into microalgae and macroalgae [2, 3]. Microalgae are represented by a wide range of single-celled autotrophic microorganisms, while macroalgae are macroscopic and multicellular organisms. Similar to plants,

✉ Jean Constantino Gomes Da Silva
jean.constantino@cear.ufpb.br

José Luiz Francisco Alves
zeluiz_alves@hotmail.com

Rosangela Lúcio Costa
rosangela.lucio@gmail.com

Seldis Fernando Dos Santos Junior
seldisjr@hotmail.com

Valdemar Francisco da Silva Filho
valdemarfilho21@hotmail.com

Regina De Fátima Peralta Muniz Moreira
regina@enq.ufsc.br

Humberto Jorge José
humberto@enq.ufsc.br

[1] Department of Chemical Engineering, Federal University of Santa Catarina, Florianópolis, SC 88040-900, Brazil

algae convert sunlight, carbon dioxide and water into biomass through photosynthesis, although algae convert more solar energy to hydrocarbon than plants. Microalgae grow faster and adapt more easily to different environments, including bioreactors, than macroalgae [1, 3]. These characteristics are present in the freshwater microalgae *Scenedesmus* sp., whose cultivation has a satisfactory cost–benefit ratio and generates high-quality biomass [4].

The energy potential of the microalgae *Scenedesmus* has been well studied, and its biological and chemical conversion is widely reported in the literature. However, there are few studies of the thermochemical conversion of *Scenedesmus* for production of biofuels through pyrolysis, specifically *Scenedesmus acuminatus*. Chen et al. [3] evaluated the torrefaction of *Scenedesmus obliquus* samples using thermogravimetric analysis under isothermal and non-isothermal conditions. Bordoloi et al. [5] characterized the products of the pyrolysis of *Scenedesmus dimorphus* and observed the presence of compounds such as n-hexane, toluene, ethyl acetate and methanol. In gas–solid reactions, such as pyrolysis, the knowledge of kinetic parameters is important for the simulation and optimization of reactors; thus, the use of thermogravimetric data associated with mathematical models is frequently used to obtain these parameters [6]. The mathematical models frequently used for the evaluation of kinetic parameters in biomass pyrolysis are isoconversional methods of Friedman, Flynn–Wall–Ozawa (FWO), Kissinger–Akahira–Sunose (KAS). Liang et al. [7] studied the pyrolysis kinetic of cellulose derived from moso bamboo and poplar using the isoconversional methods of Friedman, Flynn–Wall–Ozawa and Kissinger–Akahira–Sunose, while Ahmad et al. [8] performed an evaluation of the kinetic of *Eulaliopsis binata* pyrolysis using the methods of Flynn–Wall–Ozawa and Kissinger–Akahira–Sunose. Several other studies can be found in the literature which is used the Friedman, FWO and KAS methods for kinetic parameters evaluation [9–11]. On another hand, few studies performed the evaluation of kinetic parameters from the method of Starink are found. The method of Starink has the advantage of low relative error of the results when compared with methods of Friedman, FWO and KAS [12, 13].

This study aims to evaluate the energy potential by thermal behavior and calculate the kinetic parameters of the pyrolysis of the green microalgae *S. acuminatus* using thermogravimetric data. Moreover, the physicochemical characteristics of the green algae *S. acuminatus* were evaluated with ultimate analysis, proximate analysis, calorific value, Fourier transform infrared spectroscopy (FTIR) and BET analysis techniques.

Materials and methods

Preparation and characterization of microalgae

The green microalgae *S. acuminatus* (UTEX 415) was purchased from Culture Collection of Algae at the University of Texas (Austin, USA). The sample was dried in moisture balance (Moisture Analyzer, model MX-50, A&D Weighing, San Jose, USA) before milled through analytical mill (A 11 basic, IKA, Wilmington, USA). In the next step, the sample was sieved through a mechanical sieve shaker (Bertel, series 1.0, São Paulo, Brazil) in order to obtain a particle size of less than 106 μm (< 140 mesh) and stored in sealed vials for subsequent characterization and thermogravimetric analysis.

The microalgae biomass was characterized using proximate analysis, ultimate analysis, high-heating value calculation, Fourier transform infrared spectroscopy (FTIR) and porous structure analysis. The proximate analysis was performed according to an adapted method from ASTM E-1131 [14–17], which is determined the content of moisture, ash and volatile matter in a thermogravimetric analyzer DTG-60 Shimadzu (Kyoto, Japan), while the fixed carbon was calculated by difference. The ultimate analysis was performed with a Series II CHNS/O Analyzer, PerkinElmer 2400 (Shelton, USA), where the composition, in mass of carbon (C), hydrogen (H), nitrogen (N) and sulfur (S), was obtained experimentally. The oxygen (O) content was calculated using differences in C, H, N, S and ash. The higher heating value (HHV) was estimated according to the Channiwala and Parikh correlation, which presents absolute error of 1.45% and is needed the ultimate and proximate analysis data for HHV estimation [18]. This correlation can be applied to materials with C, H, O, N, S and ash compositions between 0.00–92.25, 0.43–25.15, 0.00–50.00, 0.00–5.60, 0.00–94.08 and 0.00–71.4%, respectively, using Eq. 1. The lower heating value (LHV) is calculated through Eq. 2, which is a relationship between HHV and LHV, and the value does not include the latent heat of vaporization of water [19].

$$\mathrm{HHV/MJ\ kg} = 0.3491\mathrm{C} + 1.1783\mathrm{H} + 0.1005\mathrm{S} - 0.1034\mathrm{O} - 0.0151\mathrm{N} - 0.0211\mathrm{Ash} \quad (1)$$

$$\mathrm{LHV/MJ\ kg} = \mathrm{HHV} - 0.2183\mathrm{H} \quad (2)$$

The specific surface area was obtained through physisorption measurement by using nitrogen (N_2) at − 196 °C in a surface area and pore size analyzer, Nova 1200e Quantachrome Instruments (Boynton Beach, USA), where the microalgae biomass was previously submitted to pretreatment at a temperature of 120 °C for 24 h. The FTIR analysis was performed by scanning at a range between 4000 and 400 cm^{-1} with a Shimadzu IRPrestige-

21 (Duisburg, Germany) using the KBr method, in a proportion of 1:100 (sample KBr) [20].

Thermogravimetric analysis

The thermogravimetric analysis of *S. acuminatus* was conducted with a Shimadzu DTG-60 analyzer (Kyoto, Japan), which has a resolution of 0.1 μg and a temperature measurement precision of ± 0.25 °C. The sample was submitted to a temperature increase from room temperature to 1000 °C at five different heating rates (10, 20, 30, 40 and 50 °C min^{-1}) under an inert gas flow of 50 mL min^{-1} (99.996% N_2), in a platinum pan. The runs were performed using an initial mass of about 10.0 ± 0.5 mg and a particle size of < 106 μm (< 140 mesh), to minimize the diffusion effects. For each run, a 60-min gas purge process was initially performed with N_2 to effectively remove the atmospheric air present within the furnace. A blank run was performed for baseline correction after each experimental run; in addition, each experiment was performed in duplicate to ensure the reproducibility of the experimental results.

Kinetic analysis of pyrolysis

Thermal decomposition kinetics is generally based on a heterogeneous conversion process in which a solid particle is converted to gas by increasing temperature. This breaks down the biomass molecule, releasing volatile compounds. The generation of volatiles is the main parameter to observe to evaluate the thermal decomposition kinetics. The kinetics are evaluated by analyzing the solid mass loss as a single-step reaction in terms of temperature (T) and conversion (α) [13]. The following fundamental rate equation describes the decomposition process:

$$\frac{d\alpha}{dt} = k(T)f(\alpha) \tag{3}$$

where $k(T)$ is the reaction constant that is a function of T (K) and $f(\alpha)$ is the reaction model of the heterogeneous conversion process. The $k(T)$ is fundamentally governed by the Arrhenius equation (Eq. 4), which is associated with the influence of temperature on the rate of the chemical reaction.

$$k(T) = Ae^{\frac{-E_a}{RT}} \tag{4}$$

where A (min^{-1}) is the frequency factor, E_a (kJ mol^{-1}) is the activation energy, and R (kJ mol^{-1} K^{-1}) is the gas constant. From the association of Eqs. 3 and 4, it is possible to obtain the following equation:

$$\frac{d\alpha}{dt} = Ae^{\frac{-E_a}{RT}}f(\alpha) \tag{5}$$

Equation 5 indicates that the decomposition process reaction is dependent on knowledge of the activated energy, frequency factor and reaction model—these parameters are called the kinetic triplet [13]. Equation 5 is not commonly used for estimating kinetic parameters, because the thermal analysis is generally performed by means of a temperature change ($dT = \nu dt$); thus, Eq. 5 becomes Eq. 6.

$$\frac{d\alpha}{dT} = \frac{A}{\nu}e^{\frac{-E_a}{RT}}f(\alpha) \tag{6}$$

where ν (°C min^{-1}) is the heating rate. The integration of Eq. 6 leads to:

$$g(\alpha) = \int_0^1 \frac{d\alpha}{f(\alpha)} = \frac{A}{\nu}\int_{T_0}^{T} e^{\frac{-E_a}{RT}}dT \equiv \frac{A}{\nu}I(E_a, T) \tag{7}$$

where $g(\alpha)$ is the integral form of the reaction model. This results in an expression that does not have an analytical solution, requiring the use of equations that represent an approximate solution to the development of isoconversional methods. Several equations have been proposed for kinetic parameters by approximation equation, including that of Doley (Eq. 8) and Murray and White (Eq. 10) approximations, which represent the methods of Flynn–Wall–Ozawa (Eq. 9) and Kissinger–Akahira–Sunose (Eq. 11), respectively [12, 13].

$$p(x) = e^{-1.0518x-5.330} \tag{8}$$

$$\log \nu = \log\left(\frac{AE_a}{Rg(\alpha)}\right) - 2.315 - 0.4567\frac{E_a}{RT} \tag{9}$$

$$p(x) = \frac{e^{-x}}{x^2} \tag{10}$$

$$\ln\left(\frac{\nu}{T^2}\right) = \ln\left(\frac{AR}{E_a g(\alpha)}\right) - \frac{E_a}{RT} \tag{11}$$

where $p(x)$ represents the integral approximation equation with $x = E_a/RT$. The estimation of E_a values by Eqs. 9 and 11 is determined using the slope of the plot of $\log(\nu)$ versus $1/T$ and $\ln(\nu/T^2)$ versus $1/T$, respectively. According to Starink [12], the use of these approximation equations (Eqs. 8 and 10) leads to inaccurate results and causes significant relative errors. For this reason, new approximate equations have been developed to reach satisfactory accuracy in the kinetic parameters values. The Starink method is an example of an isoconversional method that is highly accurate, convenient and simple to solve using linear regression analysis and the Starink approximate. This method provides significant improvement in the accuracy of the activated energy values compared to the previously mentioned methods [12, 13]. The Starink approximate and

Starink method are presented in the equations below, respectively.

$$p(x) \cong \frac{e^{-1.0008x-0.312}}{x^{1.92}} \quad (12)$$

$$\ln\left(\frac{v}{T^{1.92}}\right) = -1.0008\left(\frac{E_\alpha}{RT}\right) + \text{Constant} \quad (13)$$

The estimation of E_a values by Starink method (Eq. 13) does not require previous knowledge of the frequency factor and reaction model, which is determined using the slope of the plot of $\ln(v/T^{1.92})$ versus $1/T$. The frequency factor and reaction model are generally evaluated using the compensation effect and a master plot, respectively, due to the inability of isoconversional methods to obtain the A and $f(\alpha)$ values.

The compensation effect proposes to obtain the frequency factor values using a linear equation, which describes a relation between the activation energy and factor frequency values, as shown in Eq. 14.

$$\ln(A) = aE_a + b \quad (14)$$

where a and b are the compensation parameters. The compensation parameters are helpful for the evaluation of the $\ln(A)$ values from the E_a value obtained with the isoconversional method. These parameters are previously achieved with a linear regression between $\ln(A)_j$ and E_{aj} obtained by different reaction models (Table 1) in a model-fitting method, where the term j indicates each reaction model [21].

The reaction model is generally obtained by comparing the experimental and theoretical curves, thereby allowing the selection of the most appropriate model for the process. This method is a so-called master plot [22]. In this method, the theoretical curves are obtained from the $g(\alpha)/g(0.5)$ versus α using the $g(\alpha)$ equations presented in Table 1, while the experimental curves are obtained from experimental data in Eq. 15:

$$\frac{g(\alpha)}{g(0.5)} = \frac{p(x)}{p(x_{0.5})} \quad (15)$$

where $p(x_{0.5})$ represents the values of integral approximation when the kinetic process reaches 50% conversion, *i.e.*, $x_{0.5} = E_a/RT_{0.5}$. According to Eq. 15, the ratio of the integral function can be associated with the ratio of integral approximation, in which the experimental master plot curves are plotted as $p(x)/p(x_{0.5})$ versus α and compared with several theoretical plotted curves of $g(\alpha)/g(0.5)$ versus α.

The evaluation of kinetic parameters calculated with the isoconversional method, compensation effect and master plot was initially performed by applying E_a, A and $f(\alpha)$ values in Eq. 6 and then calculated by the numerical method of Runge–Kutta fourth-order (RK4). The results obtained by the numerical method were compared with the experimental curves using Eq. 16:

$$\text{Fit} = \sum_{i=1}^{N} \frac{\sqrt{\left[(d\alpha/dt)_{exp} - (d\alpha/dt)_{calc}\right]^2 / N}}{(d\alpha/dt)_{exp}^{highest}} \quad (16)$$

where N is the number of experimental data points used, $(d\alpha/dt)_{exp}$ is the experimental values measured, and $(d\alpha/dt)_{calc}$ is the differential value calculated. The kinetic parameters and simulated curves were calculated through Microsoft Excel 365.

Results and discussion

Characterization

Table 2 shows the physiochemical characterization obtained for *S. acuminatus* in this study and observation data reported in the literature about other microalgae, such as *Scenedesmus* sp., *Scenedesmus almeriensis*, *S. dimorphus*, *Dunaliella salina*, *Chlorella vulgaris* and *Tetraselmis suecica* [5, 23–27].

The proximate analysis shows a moisture content of 3.34%, where the content is between the values found for other microalgae as shown in Table 2 (0.08–4.59%). According to García et al. [28], a low moisture content (< 10%) is required to increase the amount of useful energy in a combustible solid when applied in thermochemical systems, because evaporation is an endothermic process. Table 2 indicates different values of ash content among the microalgae, where the content varies from 21.65 to 7.20%. For *S. acuminatus,* a value of 9.34% was obtained, which is low compared to the lignocellulosic biomass found in the literature such as for rice husks (13.3%), sorghum (17.0%), straw pellets (9.8%) and grapevine waste (13.3%) [28, 29]. Table 2 shows a relatively high content of volatile matter and low content of fixed carbon for *S. acuminatus* among the microalgae. This result indicates that the microalgae used in this study release a high amount of combustible (C_xH_y, CO and H_2) and non-combustible (CO_2, SO_2, NO_x and H_2O) gases during pyrolysis.

The calorific value estimated with the Channiwala and Parikh correlation showed a similar value of HHV between the *S. acuminatus* (20.58 MJ kg^{-1}) and the other microalgae as noted in Table 2. The HHV of *S. acuminatus* was higher than that found for lignocellulosic biomass such as bagasse sugarcane (16.4 MJ kg^{-1}), rice husks (16.7 MJ kg^{-1}), corn stalks (15.81 MJ kg^{-1}) and pistachio shells (17.47 MJ kg^{-1}) [29–31]. This HHV can be

Table 1 List of reaction models often used in solid-state reaction kinetics

Model	Mechanism	$g(\alpha)$	$f(\alpha)$
P2	Power law	$\alpha^{1/2}$	$2\alpha^{1/2}$
P3	Power law	$\alpha^{1/3}$	$3\alpha^{2/3}$
P4	Power law	$\alpha^{1/4}$	$4\alpha^{3/4}$
P2/3	Power law	$\alpha^{3/2}$	$2/3\alpha^{-1/2}$
F1	First-order reaction	$-\ln(1-\alpha)$	$1 - \alpha$
F2	Second-order reaction	$(1-\alpha)^{-1}-1$	$(1 - \alpha)^2$
F3	Third-order reaction	$(1/2)\left[(1-\alpha)^{-2}-1\right]$	$(1 - \alpha)^3$
R2	Contracting cylinder (contracting area)	$1-(1-\alpha)^{1/2}$	$2(1-\alpha)^{1/2}$
R3	Contracting sphere (contracting volume)	$1-(1-\alpha)^{1/3}$	$3(1-\alpha)^{2/3}$
D1	One-dimensional diffusion	α^2	$1/2\alpha^{-1}$
D2	Two-dimensional diffusion	$(1-\alpha)\ln(1-\alpha)+\alpha$	$[-\ln(1-\alpha)]^{-1}$
D3	Three-dimensional diffusion	$\left[1-(1-\alpha)^{1/3}\right]^2$	$3/2(1-\alpha)^{2/3}\left[1-(1-\alpha)^{1/3}\right]^{-1}$
D4	Ginstling-Brounshtein	$1-(2/3)\alpha-(1-\alpha)^{2/3}$	$3\left[2\left((1-\alpha)^{-1/3}-1\right)\right]^{-1}$
A2	Avrami-Erofeev	$[-\ln(1-\alpha)]^{1/2}$	$2(1-\alpha)[-\ln(1-\alpha)]^{1/2}$
A3	Avrami-Erofeev	$[-\ln(1-\alpha)]^{1/3}$	$3(1-\alpha)[-\ln(1-\alpha)]^{2/3}$
A4	Avrami-Erofeev	$[-\ln(1-\alpha)]^{1/4}$	$4(1-\alpha)[-\ln(1-\alpha)]^{3/4}$

associated with the low moisture and ash content found in the proximate analysis, as well as the chemical composition of the microalgae. The energy potential of green microalgae *S. acuminatus* in thermal conversion processes can be compared to solid fuels which are widely applied on bioenergy production, such as wood sawdust, where presents an HHV between 18 and 19 MJ kg^{-1}. Unlike the lignocellulosic biomass, microalgae are chemically composed of lipids, carbohydrates, proteins and others nutrients and thus have different carbon, hydrogen and oxygen contents. This different composition provides a low oxygen content and a higher carbon and hydrogen content in microalgae than in lignocellulosic biomass. Several types of lignocellulosic biomass were evaluated by Garcia et al. [32] who noted an average of 44.59, 48.30 and 5.71% for carbon, oxygen and hydrogen content, respectively. According to the Channiwala and Parikh correlation, a high carbon and hydrogen content contribute positively to the HHV, while a high oxygen content contributes negatively. Low levels of sulfur in fuels are preferable due to the low probability of this element generates sulfur dioxide (SO_2) in the thermochemical system. Sulfur can damage equipment from condensation on the walls of equipment; besides, this can be associated with inorganic compounds and generated incrustations or released together with the exhaust gases. Therefore, the application of microalgae *S. acuminatus* must be carried out with attention due to the high sulfur presence (1.39%) when compared to same types of biomass such as agro-industrial residues [17], sewage sludge [15], meat industry wastes [33], however, comparable to tomato plant waste and holm oak branch chips [32]. The nitrogen content in the microalgae sample presented 5.93%, probably due to a high content of proteins. The presence of nitrogen can cause NO_x emissions when using thermochemical systems that work at temperatures above 500 °C [34].

Figure 1 shows the FTIR spectrum for *S. acuminatus*, while the Table 3 shows the main bands. The band at 3410 cm^{-1} corresponds to hydroxyl groups (O–H) stretching in water, acid groups and alcohol groups. This band can also be associated with N–H stretching vibrations in primary amides. The bands at 2930 and 2845 cm^{-1} are often found in methylene groups, which, respectively, represent the asymmetric and symmetric C–H stretching vibration. These bands can be associated with $–CH_2$ stretching in lipids, which was observed by Difusa et al. [35] after they conducted a lipid extraction of microalgae *Chloromonas* sp. The band at 2360 cm^{-1} represents the overlapping between the O–H and NH_3^+ stretching vibrations. The band at 1656 cm^{-1} corresponds to stretching vibrations of a strong carbonyl group (C=O) in primary amides [36]. The bands at 1543 and 1240 cm^{-1} represent an amide II band that can be associated with the interaction between the N–H bending and C–N stretching of a C–N–H group in acyclic amides, while the band at 1406 cm^{-1} represents the $–CH_2$ bending of lipids [35, 37]. The infrared region at 1017–1022 cm^{-1} is associated with the strong C–O–C symmetric stretching of an ether group. The band at

Table 2 Physicochemical characteristic of *Scenedesmus acuminatus* and different microalgae from studies

Reference	*Scenedesmus acuminatus* This work	*Scenedesmus* sp. Kim [24]	*Scenedesmus almeriensis* López-González [25]	*Scenedesmus dimorphus* Bordoloi [5]	*Dunaliella salina* Gong [27]	*Chlorella vulgaris* Chen [23]	*Tetraselmis suecica* Tahmasebi et al. [26]
Proximate analysis/%							
Moisture	3.34[a]	4.59	2.90	0.083[b]	4.00[b]	–	4.27
Volatile matter	81.63[b]	75.33	67.90	51.45[b]	76.30[b]	55.37	58.31
Fixed carbon	9.03[b,c]	12.78	9.70	31.13[b,c]	12.50[b]	34.35	15.77
Ash	9.34[b]	7.30	19.40	17.33[b]	7.20[b]	10.28	21.65
Ultimate analysis/%							
Carbon (C)	46.49[b]	50.00	41.90[b]	52.60[b]	48.10[b]	47.84	27.72
Hydrogen (H)	6.48[b]	7.11	6.70[b]	6.21[b]	7.10[b]	6.41	4.59
Nitrogen (N)	5.93[b]	7.25	5.90[b]	8.75[b]	9.40[b]	9.01	4.70
Sulfur (S)	1.39[b]	0.54	0.80[b]	–	0.90[b]	1.46	1.11
Oxygen (O)	30.37[b,c]	30.70	44.70[b]	31.92[b,c]	23.30[b,c]	25.00	40.23
Heating value							
HHV/MJ kg^{-1}	20.58	21.10	–	19.00	21.20	–	–
LHV/MJ kg^{-1}	19.26	–	–	–	–	21.88[b]	–
Porous structure							
BET surface area/m^2 g^{-1}	0.267	–	–	–	–	–	–
Pore volume[d]/cm^3 g^{-1}	0.00108	–	–	–	–	–	–

[a]Wet basis

[b]Dry basis

[c]Calculated by difference

[d]Total pore volume at $P/P_0 = 0.99$

530 cm^{-1} represents the C–N–S bending of organic sulfur compounds [37].

Thermogravimetric analysis

Figure 2 shows the thermogravimetric (TG) and differential thermogravimetric (DTG) curves of the pyrolysis of *S. acuminatus* under an inert atmosphere at a heating rate of 10, 20, 30, 40 and 50 °C min^{-1}. The DTG curves indicate that the thermal behavior of microalgae presents different stages of mass loss. For the 10 °C min^{-1}, an initial stage between room temperature and 125 °C occurs and is associated with the dehydration of the microalgae sample [38]. This dehydration is represented by a mass loss of 2.7% and a maximum mass loss rate of 0.51% min^{-1} close to a temperature of 78 °C. Figure 2 shows that the pyrolysis of *S. acuminatus* begins after dehydration, when there is a breakdown of chemical bonds in proteins, lipids, carbohydrates and others compounds in the microalgae and the formation of light hydrocarbons. From the DTG data, the pyrolysis of *S. acuminatus* takes place between the temperatures of 125 and 504 °C, where two peak temperatures are noticed in different temperature ranges. The first temperature range of pyrolysis, from 125 to 392 °C, shows a mass loss of 44.4% and a maximum mass loss rate of 3.81% min^{-1} occurring at around the temperature 301 °C. This thermal decomposition region was also observed by Chen et al. [3] and Sanchez-Silva et al. [38] in samples of *S. obliquus* and *Nannochloropsis gaditana*, respectively, which was represented by the decomposition of carbohydrates and proteins in the microalgae. The second temperature range is between 392 and 504 °C, which is noted a mass loss of 16.0% and a maximum mass loss rate of 2.34% min^{-1} occurring at around 452 °C. A similar DTG profile was observed by Bordoloi et al. [5] for *S. dimorphus*, where the presence of a weak peak in the mass loss rate was associated with lipid decomposition. After these events, thermal decomposition occurs slowly in the temperature range from 504 to 900 °C with a mass loss of 10.22%, associated with the slow decomposition of the carbonaceous product formed after the breakdown of the chemical bonds of the proteins, carbohydrates and lipids in the microalgae [5, 25]. The TG curve indicates that the carbonaceous product represents 20.7% of the initial sample mass.

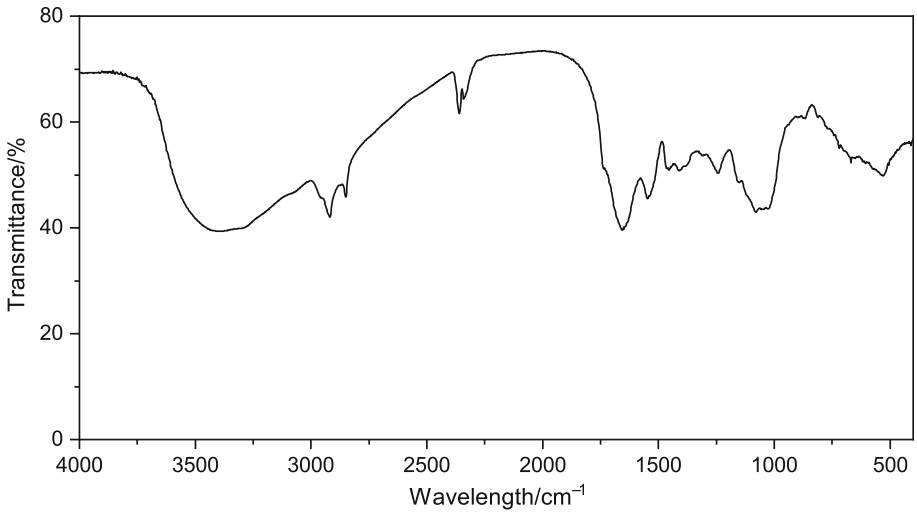

Fig. 1 Fourier transform infrared spectroscopy spectrum of *Scenedesmus acuminatus*

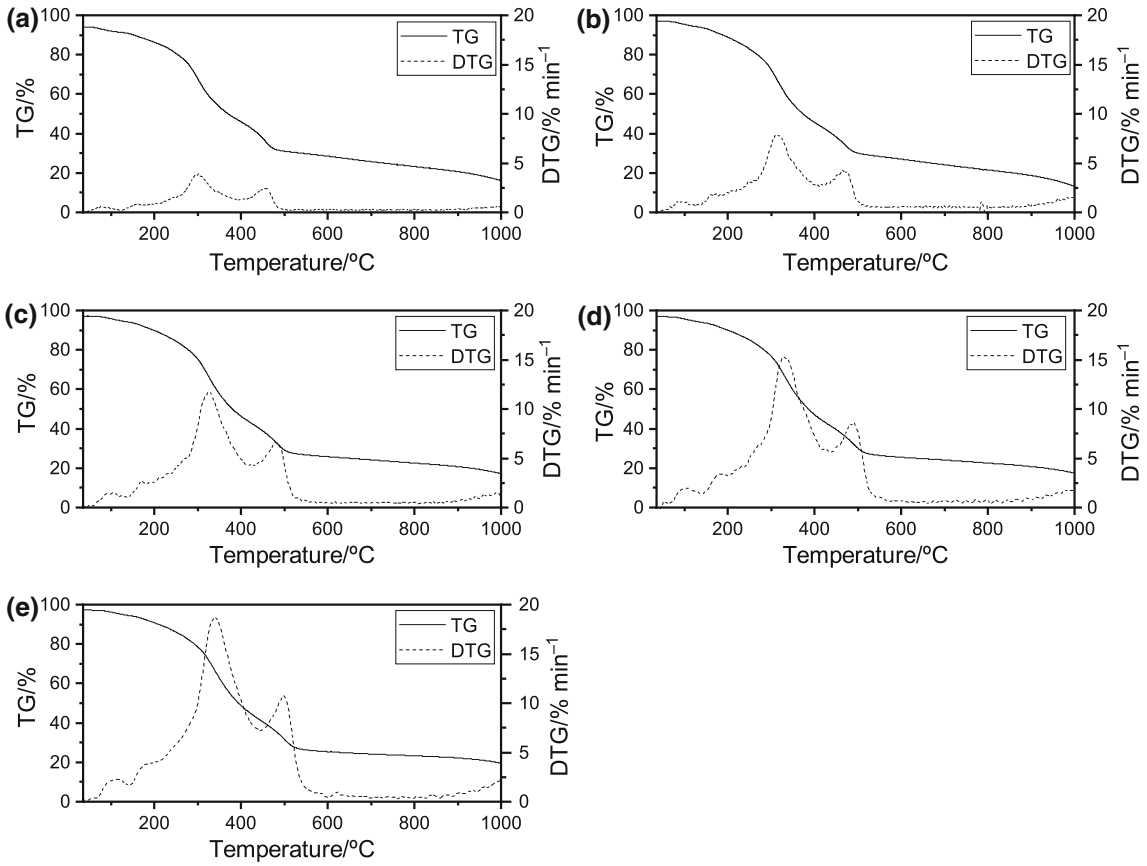

Fig. 2 TG (*solid line*) and DTG (*dot line*) curves from pyrolysis process of *Scenedesmus acuminatus* at **a** 10 °C min^{-1}, **b** 20 °C min^{-1}, **c** 30 °C min^{-1}, **d** 40 °C min^{-1}, and **e** 50 °C min^{-1} under nitrogen atmosphere

Kinetic study

The thermal behavior of *S. acuminatus* (Fig. 2) indicates that the pyrolysis of the microalgae occurs in two stages (multi-step). Therefore, the use of the isoconversional methods for kinetic study must be conducted to evaluate each stage separately. Thus, the evaluation of the kinetic parameters was performed using the thermogravimetric data in the temperature ranges presented in Table 4, where stage I represents the decomposition of carbohydrates and proteins and stage II represents the lipids decomposition. Thus, Fig. 3 shows the results of $E_{a\alpha}$ calculated from

thermogravimetric data at each mass loss region for methods of Flynn–Wall–Ozawa (FWO), Kissinger–Akahira–Sunose (KAS) and Starink. The $E_{a\alpha}$ results present a higher linear correlation coefficient ($R^2 \geq 0.9485$) for the conversion range of $0.05 \leq \alpha \leq 0.95$.

Figure 3 shows the relationship between the activation energy and conversion ($E_{a\alpha}$) in the conversion range of $0.05 \leq \alpha \leq 0.95$. It can be seen that in stage I the initial values of $E_{a\alpha}$ estimated by the isoconversional method are significantly high than those for the conversion process in this stage, where the $E_{a\alpha}$ values were between 148.8–104.2, 149.1–99.0 and 149.5–99.6 kJ mol^{-1}, respectively, for methods of FWO, KAS and Starink. This behavior at initial value of $E_{a\alpha}$ can indicate that the temperature is not high enough to break down the chemical bonds in the molecules. For stage I, the average activated energy (E_{a0}) was 110.7, 106.8 and 107.1 kJ mol^{-1}, for methods of FWO, KAS and Starink, respectively. The initial step in stage II has $E_{a\alpha}$ values approximately similar to the end of stage I; however, there is a gradual increase in $E_{a\alpha}$ values between the conversion range of $0.05 \leq \alpha \leq 0.7$, which presented an increase of 105.5–110.89 to 144.8–149.7 kJ mol^{-1}. After conversion 0.7, there was a small drop in $E_{a\alpha}$ values to 133.7–139.5 kJ mol^{-1} in the conversion at 0.95. In stage II, the activation energy had an E_{a0} value of 137.2, 132.0 and 132.6 kJ mol^{-1}, respectively. Figure 3c, d shows a low relative error for methods of KAS and Starink, when compared with the average, which exhibited a relative error less than 1% for each stage. However, for simulation curves, it is noted that the Starink's method shows a better application due to its relative error of 0.07 and 0.10% for stages I and II, respectively, while the KAS's method showed a relative error of 0.38 and 0.36% for stages I and II, respectively.

The average activation energy for stage I is lower than that for stage II. According to Hu et al. [39], this implies that the pyrolysis in stage I occurs more easily than in stage II. According to Vo et al. [40], the pyrolysis costs reduces the value of the average activation energy reduces. Thus, considering stage I the main stage of decomposition due to the gaseous yield (Table 4), *S. acuminatus* is better applicable to pyrolysis than microalgae such as *Chlorella pyrenoidosa* (143.71 kJ mol^{-1}) and *Aurantiochytrium* sp. (118.54 kJ mol^{-1}), biomass such as sugarcane bagasse (124.54 kJ mol^{-1}) and some water waste such as *Baijiu Diuzao* (150.98–152.86 kJmol^{-1}) [11, 39–41].

The typical linear fit between ln ($v\ T^{-1.92}$) versus $1/T$, which was obtained by the Starin isoconversional method (Eq. 13) for the conversion range of $0.1 \leq \alpha \leq 0.9$, is shown in Fig. 4. Figure 4 shows nearly parallel behavior between the straight line of the linear fit and the satisfactory correlation coefficients for the two stages ($R^2_{\text{stageI}} \geq 0.9486$ and $R^2_{\text{stageII}} \geq 0.9806$). In stage I (Fig. 4a), a larger gap is observed between the straight line at conversions 0.1 and 0.2 and is associated with the pyrolysis step in which the conversion occurs more slowly. The initial pyrolysis step has a low mass loss rate, as observed in Fig. 2, thus requiring more energy to break down the chemical bonds in the microalgae. Subsequently, between the conversions of $0.3 \leq \alpha \leq 0.9$, the temperatures become sufficient for the effective pyrolysis reaction; in this way, the decomposition occurs with higher mass loss rates and a small variation of activation values [31]. Unlike stage I, stage II (Fig. 4b) shows similar behavior between the straight lines over the entire conversion range.

The inability to estimate the values of the frequency factor and the reaction model by isoconversional methods are the main reasons for the use of methods such as the compensation effect and the master plot method [13]. Thus, Fig. 5 presents the linear fit obtained by the compensation effect and the master plot curves for *S. acuminatus* pyrolysis. Figure 5a indicates a satisfactory linear fit for the two stages, with regression coefficients (R^2) of 0.9648 and 0.9989 for stages I and II, respectively. This regression coefficient demonstrates a good approximation with the A_α values calculated by the linear equation (Eq. 14). The compensation parameters a and b obtained for stage I were, respectively, 0.2283 and − 3.4228, and for stage II were 0.1617 and − 1.4691. Substituting the values of the compensation parameters in Eq. 14, an average frequency factor (A_0) of 13.56×10^8 min^{-1} and 4.47×10^8 min^{-1} is obtained for stages I and II, respectively.

Figure 5b shows the overlapping between the experimental and theoretical curves of the master plot method based on the integral form of kinetic data for *S. acuminatus*. Initially, it is noted in Fig. 5b that the experimental data do not perfectly match the theoretical curves, which indicates the occurrence of different reaction mechanisms

Table 3 Band assignments from FTIR spectrum of *Scenedesmus acuminatus*

Wavelength/cm^{-1}	Assignment	Comments
3410	ν(O–H); ν(N–H)	Amide I
2920	ν_s(–CH$_2$)	Lipid
2845	ν_{as}(–CH$_2$)	Lipid
2360	ν(O–H); ν(N–H)	–
1656	ν(C=O)	Amide I
1543	Interaction ν(C–N) and δ(N–H)	Amide II
1406	δ(–CH$_2$)	Lipid
1240	Interaction ν(C–N) and δ(N–H)	Amide II
1076–1022	ν_s(C–O–C)	–
530	δ(C–N–S)	–

Table 4 Temperature range and mass loss for pyrolysis stages of *Scenedesmus acuminatus*

Heating rate/°C min^{-1}	Stage 1			Stage 2		
	T_i/°C	T_f/°C	Mass loss$^{d.b.}$/%	T_i/°C	T_f/°C	Mass loss$^{d.b.}$/%
10	125	392	58.49	392	504	21.08
20	125	411	61.06	411	522	18.16
30	125	422	65.87	422	541	20.43
40	125	439	68.38	439	551	18.84
50	125	447	70.52	447	569	19.73

T_i Temperature initial, T_f temperature final and *d.b.* dry basis

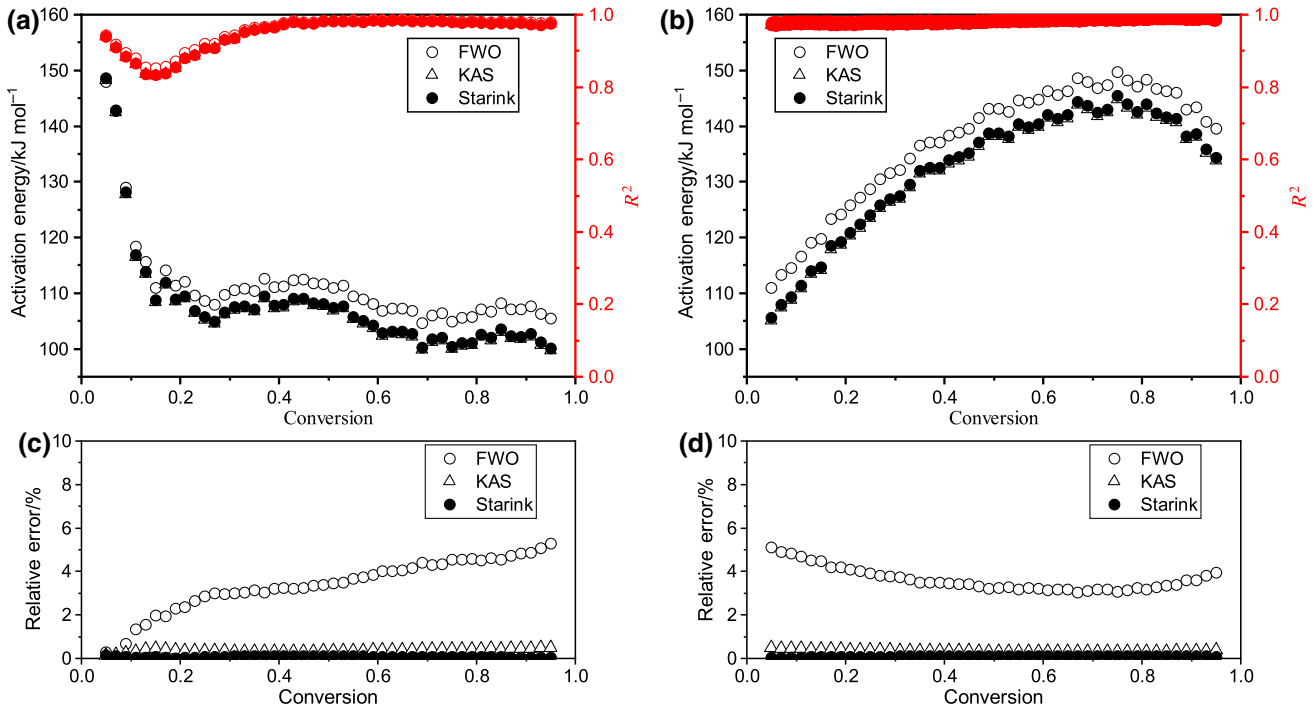

Fig. 3 Activation energy values estimated for the pyrolysis of *Scenedesmus acuminatus* by methods of FWO, KAS and Starink for stages I (**a**) and II (**b**) and the relative error of methods for stages I (**c**) and II (**d**)

due to the complex decomposition process of the microalgae. On the other hand, it is possible to select the reaction mechanism through the theoretical curve that best represents the experimental results. Therefore, the reaction mechanisms selected for the pyrolysis in stages I and II were the second-order reaction (F2) and contracting volume (R3), respectively. A similar reaction mechanism was observed by Ye et al. [11] in water waste sample (*B. Diuzao*), where a *n*-order reaction and contracting geometry showed a better fit for experimental data on a similar temperature range for stages I and II, respectively.

Based on the kinetic parameter data estimated by the Starink isoconversional method, compensation effect and master plot (Table 5), it is possible to describe an equation for the pyrolysis of *S. acuminatus*. Thus, using Eq. 5, the microalgae decomposition process in this study can be described by the equation below.

$$\left(\frac{d\alpha}{dt}\right)_{\text{pyrolysis}} \begin{cases} \left(\frac{d\alpha}{dt}\right)_{\text{StageI}} = \eta_{\text{I}}(13.56\times10^{8})e^{107,085.5/RT}(1-\alpha)^{2} \\ \left(\frac{d\alpha}{dt}\right)_{\text{StageII}} = \eta_{\text{II}}(4.74\times10^{8})e^{132,625.2/RT}\left[3(1-\alpha)^{2/3}\right] \end{cases} \quad (17)$$

Equation 17 shows that the overall pyrolysis process is described as the sum of the pyrolysis of each stage, where η is the average of the mass loss fraction for each stage (Table 4). Equation 17 allows estimating the conversion rate curves and comparing them with the experimental data. To calculate (simulate) the curves, from Eq. 17, it is necessary to use a numerical method due to the relationship between the conversion and temperature ($\alpha = \alpha(T)$). Thus, the classical numerical method of Runge–Kutta fourth-order (RK4) provides the curves shown in Fig. 6.

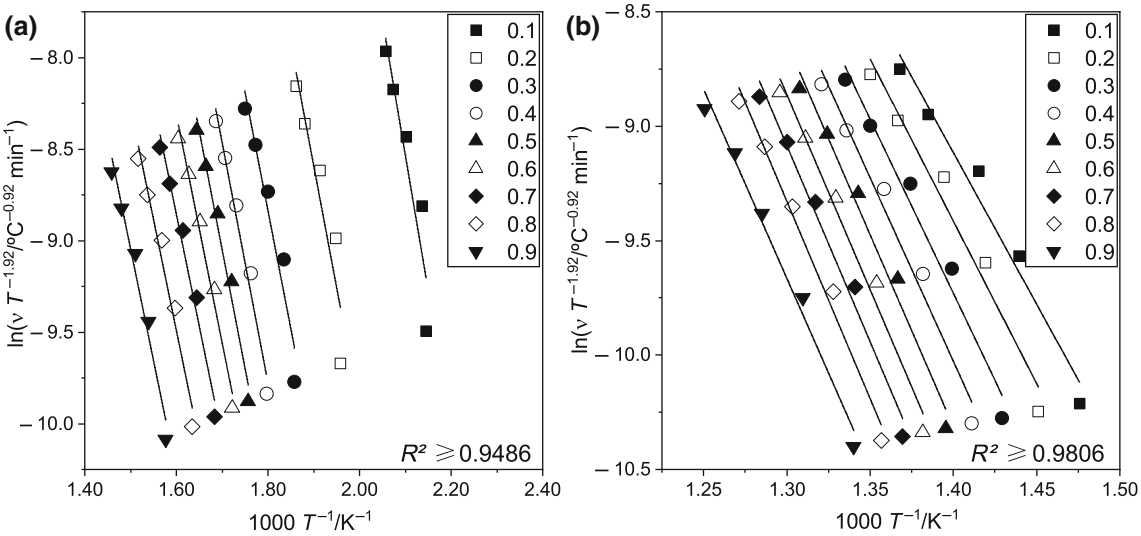

Fig. 4 Linear fit of $\ln(v\ T^{-1.92})$ versus 1000 T^{-1} for pyrolysis stages I (**a**) and II (**b**)

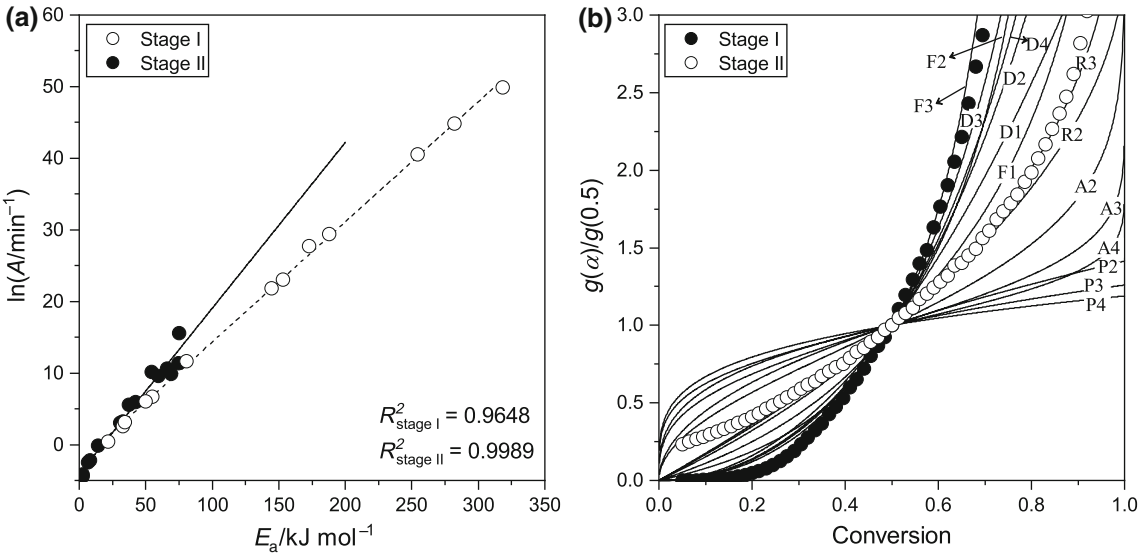

Fig. 5 **a** Linear fit of compensation effect and **b** overlapping between experimental and theoretical master plot curves

Figure 6 shows the overlapping of the dα/dt versus T curves for the experimental and calculated data, indicating similar behavior between the experimental and calculated curves. On the other hand, other regions have a low adjustment. In Fig. 6, the curves calculated at temperatures below 200 °C do not show a value for the conversion rate, whereas the experimental curves indicate a conversion rate of $\sim$ 0.5 min^{-1}. This behavior is due to the kinetic parameters calculated using isoconversional methods to provide a curve that represents only a single-step mechanism, in which the region with high conversion rates is best represented. In stage I, the peak temperatures exhibited a temperature difference of $\pm$ 10 °C between the experimental and calculated data. At this stage, the calculated conversion rate data presented higher results than the experimental data, due to the compensation of the area, which was not demonstrated at temperatures below 200 °C. Unlike stage I, the curves calculated for stage II had a satisfactory fit for all the heating rates. The conversion rate curves have a regression coefficient of 0.8673, 0.8610, 0.8760, 0.8785 and 0.8847 for the heating rates of 10, 20, 30, 40 and 50 °C min^{-1}. These results are satisfactory for application in thermochemical systems and represent a good option for predetermining thermal decomposition curves.

Table 5 Kinetic parameters obtained from isoconversional method, compensation effect and master plot for the pyrolysis of *Scenedesmus acuminatus*

	Stage I	Stage II
Isoconversional method		
E_{a0}/kJ mol^{-1}	107.1	132.6
R^2	0.9486	0.9806
Compensation effect		
a	0.2283	0.1617
b	− 3.4228	− 1.4691
R^2	0.9648	0.9989
A_0/min^{-1}	13.56 × 10^8	4.47 × 10^8
Master plot		
$f(\alpha)$	F2	R3

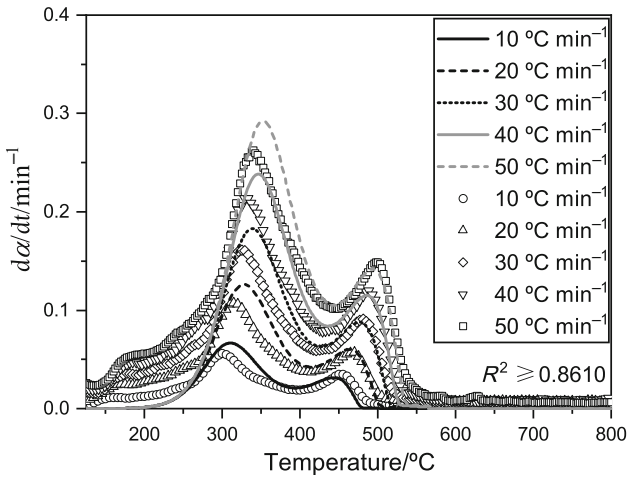

Fig. 6 Comparison of experimental (*symbol*) and calculated (*line*) curves for the pyrolysis of *Scenedesmus acuminatus* at heating rate of 10, 20, 30, 40 and 50 °C min^{-1}

Conclusions

The physicochemical characteristics and pyrolysis kinetics were evaluated for *S. acuminatus*, for which there are few reports in the literature about its behavior. This microalgae revealed to have good applicability for thermal systems when compared with other microalgae and biomass. Its thermal behavior was divided into two stages to represent the decomposition of carbohydrates and proteins (stage I) and lipids (stage II). The Starink's method shows a better application for simulation curves due to the low relative error, when compared with the methods of FWO and KAS. The comparison between the experimental and calculated curves showed the satisfactory applicability of kinetic parameters calculated by using the isoconversional method of Starink, compensation effect and master plot. These data are important for the operation and modeling of thermal systems showing that the microalgae biomass can be a sustainable and low-cost resource. The microalgae biomass pyrolysis offers a cleanest process to obtain the bioenergy stored in the solid fuel.

Acknowledgements The authors are grateful for the financial support to this research from the National Council for Scientific and Technological Development (CNPq) and the Coordination for the Improvement of Higher Education Personnel (CAPES).

References

1. Saber M, Nakhshiniev B, Yoshikawa K. A review of production and upgrading of algal bio-oil. Renew Sustain Energy Rev. 2016;58:918–30.
2. Suganya T, Varman M, Masjuki HH, Renganathan S. Macroalgae and microalgae as a potential source for commercial applications along with biofuels production: a biorefinery approach. Renew Sustain Energy Rev. 2016;55:909–41.
3. Chen W-H, Wu Z-Y, Chang J-S. Isothermal and non-isothermal torrefaction characteristics and kinetics of microalga *Scenedesmus obliquus* CNW-N. Bioresour Technol. 2014;155:245–51.
4. Chandra TS, Deepak RS, Kumar MM, Mukherji S, Chauhan VS, Sarada R, Mudliar SN. Evaluation of indigenous fresh water microalga *Scenedesmus obtusus* for feed and fuel applications: effect of carbon dioxide, light and nutrient sources on growth and biochemical characteristics. Bioresour Technol. 2016;207:430–9.
5. Bordoloi N, Narzari R, Sut D, Saikia R, Chutia RS, Kataki R. Characterization of bio-oil and its sub-fractions from pyrolysis of *Scenedesmus dimorphus*. Renew Energy. 2016;98:245–53.
6. Park WC, Atreya A, Baum HR. Experimental and theoretical investigation of heat and mass transfer processes during wood pyrolysis. Combust Flame. 2010;157:481–94.
7. Liang F, Zhang T, Xiang H, Yang X, Hu W, Mi B, Liu Z. Pyrolysis characteristics of cellulose derived from moso bamboo and poplar. J Therm Anal Calorim. 2018;132:1359–65.
8. Ahmad MS, Mehmood MA, Ye G, Al-Ayed OS, Ibrahim M, Rashid U, Luo H, Qadir G, Nehdi IA. Thermogravimetric analyses revealed the bioenergy potential of *Eulaliopsis binata*. J Therm Anal Calorim. 2017;130:1237–47.
9. Thakur LS, Varma AK, Mondal P. Analysis of thermal behavior and pyrolytic characteristics of vetiver grass after phytoremediation through thermogravimetric analysis. J Therm Anal Calorim. 2018;131:3053–64.
10. Wang X, Wang X, Qin G, Chen M, Wang J. Comparative study on pyrolysis characteristics and kinetics of lignocellulosic biomass and seaweed. J Therm Anal Calorim. 2018;132:1317–23.
11. Ye G, Luo H, Ren Z, Ahmad MS, Liu C-G, Tawab A, Al-Ghafari AB, Omar U, Gull M, Mehmood MA. Evaluating the bioenergy potential of Chinese liquor-industry waste through pyrolysis, thermogravimetric, kinetics and evolved gas analyses. Energy Convers Manag. 2018;163:13–21.
12. Starink MJ. The determination of activation energy from linear heating rate experiments: a comparison of the accuracy of isoconversion methods. Thermochim Acta. 2003;404:163–76.
13. Vyazovkin S, Burnham AK, Criado JM, Pérez-maqueda LA, Popescu C, Sbirrazzuoli N. Thermochimica Acta ICTAC Kinetics Committee recommendations for performing kinetic computations on thermal analysis data. Thermochim Acta. 2011;520:1–19.

14. ASTM. E1131-08: Standard test method for compositional analysis by thermogravimetry. Annu B ASTM Stand. West Conshohocken: ASTM International; 2014. p. 1–6.
15. Batistella L, Silva V, Suzin RC, Virmond E, Althoff CA, Moreira RFPM, José HJ. Gaseous emissions from sewage sludge combustion in a moving bed combustor. Waste Manag. 2015;46:430–9.
16. da Silva JCG, Alves JLF, de Galdino WVA, Andersen SLF, de Sena RF. Pyrolysis kinetic evaluation by single-step for waste wood from reforestation. Waste Manag. 2018;72:265–73.
17. Pacioni TR, Soares D, Di Domenico M, Rosa MF, Moreira RFPM, José HJ. Bio-syngas production from agro-industrial biomass residues by steam gasification. Waste Manag. 2016;58:221–9.
18. Channiwala SA, Parikh PP. A unified correlation for estimating HHV of solid, liquid and gaseous fuels. Fuel. 2002;81:1051–63.
19. Kan T, Strezov V, Evans TJ. Lignocellulosic biomass pyrolysis: a review of product properties and effects of pyrolysis parameters. Renew Sustain Energy Rev. 2016;57:1126–40.
20. ASTM. D2702-05: standard practice for rubber chemicals—determination of infrared absorption characteristics. Annu B ASTM Stand. West Conshohocken: ASTM International; 2016. p. 4.
21. Khawam A, Flanagan DR. Solid-state kinetic models: basics and mathematical fundamentals. J Phys Chem B. 2006;110:17315–28.
22. Gotor FJ, Criado JM, Malek J, Koga N. Kinetic analysis of solid-state reactions: the universality of master plots for analyzing isothermal and nonisothermal experiments. J Phys Chem A. 2000;104:10777–82.
23. Chen C, Lu Z, Ma X, Long J, Peng Y, Hu L, Lu Q. Oxy-fuel combustion characteristics and kinetics of microalgae *Chlorella vulgaris* by thermogravimetric analysis. Bioresour Technol. 2013;144:563–71.
24. Kim SW, Koo BS, Lee DH. A comparative study of bio-oils from pyrolysis of microalgae and oil seed waste in a fluidized bed. Bioresour Technol. 2014;162:96–102.
25. López-González D, Fernandez-Lopez M, Valverde JL, Sanchez-Silva L. Pyrolysis of three different types of microalgae: kinetic and evolved gas analysis. Energy. 2014;73:33–43.
26. Tahmasebi A, Kassim MA, Yu J, Bhattacharya S. Thermogravimetric study of the combustion of *Tetraselmis suecica* microalgae and its blend with a Victorian brown coal in O_2/N_2 and O_2/CO_2 atmospheres. Bioresour Technol. 2013;150:15–27.
27. Gong X, Zhang B, Zhang Y, Huang Y, Xu M. Investigation on pyrolysis of low lipid microalgae *Chlorella vulgaris* and *Dunaliella salina*. Energy Fuels. 2014;28:95–103.
28. García R, Pizarro C, Lavín AG, Bueno JL. Spanish biofuels heating value estimation. Part II: proximate analysis data. Fuel. 2014;117:1139–47.
29. Yu Y, Yang Y, Cheng Z, Blanco PH, Liu R, Bridgwater AV, Cai J. Pyrolysis of rice husk and corn stalk in auger reactor. 1. Characterization of char and gas at various temperatures. Energy Fuels. 2016;30:10568–74.
30. Boumanchar I, Chhiti Y, Alaoui FEM, El Ouinani A, Sahibed-Dine A, Bentiss F, Jama C, Bensitel M. Effect of materials mixture on the higher heating value: case of biomass, biochar and municipal solid waste. Waste Manag. 2017;61:78–86.
31. da Silva JCG, Alves JLF, Galdino WVA, Moreira RFPM, José HJ, de Sena RF, Andersen SLF. Combustion of pistachio shell: physicochemical characterization and evaluation of kinetic parameters. Environ Sci Pollut Res. 2017;1:1–10.
32. García R, Pizarro C, Lavín AG, Bueno JL. Characterization of Spanish biomass wastes for energy use. Bioresour Technol. 2012;103:249–58.
33. de Sena RF, Claudino A, Moretti K, Bonfanti ÍCPP, Moreira RFPM, José HJ. Biofuel application of biomass obtained from a meat industry wastewater plant through the flotation process—a case study. Resour Conserv Recycl. 2008;52:557–69.
34. Zhan H, Yin X, Huang Y, Yuan H, Xie J, Wu C, Shen Z, Cao J. Comparisons of formation characteristics of NO_x precursors during pyrolysis of lignocellulosic industrial biomass wastes. Energy Fuels. 2017;31:9557–67.
35. Difusa A, Mohanty K, Goud VV. The chemometric approach applied to FTIR spectral data for the analysis of lipid content in microalgae cultivated in different nitrogen sources. Biomass Convers Biorefinery. 2016;6:427–33.
36. Jiang Y, Yoshida T, Quigg A. Photosynthetic performance, lipid production and biomass composition in response to nitrogen limitation in marine microalgae. Plant Physiol Biochem. 2012;54:70–7.
37. Silverstein RM, Webster FX, Kiemle DJ. Spectrometric identification of organic compounds. 7th ed. New York: Wiley; 2005.
38. Sanchez-Silva L, López-González D, Garcia-Minguillan AM, Valverde JL. Pyrolysis, combustion and gasification characteristics of *Nannochloropsis gaditana* microalgae. Bioresour Technol. 2013;130:321–31.
39. Hu M, Chen Z, Guo D, Liu C, Xiao B, Hu Z, Liu S. Thermogravimetric study on pyrolysis kinetics of *Chlorella pyrenoidosa* and bloom-forming cyanobacteria. Bioresour Technol. 2015;177:41–50.
40. Vo TK, Ly HV, Lee OK, Lee EY, Kim CH, Seo J-W, Kim J, Kim S-S. Pyrolysis characteristics and kinetics of microalgal *Aurantiochytrium* sp. KRS101. Energy. 2017;118:369–76.
41. Zanatta ER, Reinehr TO, Awadallak JA, Kleinübing SJ, dos Santos Junior SF, Bariccatti RA, Arroyo PA, da Silva EA. Kinetic studies of thermal decomposition of sugarcane bagasse and cassava bagasse. J Therm Anal Calorim. 2016;125:437–45.